Acute growth hormone administration induces antidiuretic and antinatriuretic effects and increases phosphorylation of NKCC2

Henrik Dimke, Allan Flyvbjerg, Soline Bourgeois, Klaus Thomsen, Jørgen Frøkiær, Pascal Houillier, Søren Nielsen and Sebastian Frische

Am J Physiol Renal Physiol 292:F723-F735, 2007. First published 24 October 2006;
doi:10.1152/ajprenal.00276.2006

AJP - Renal Physiology publishes original manuscripts on a broad range of subjects relating to the kidney, urinary tract, and their respective cells and vasculature, as well as to the control of body fluid volume and composition. It is published 12 times a year (monthly) by the American Physiological Society, 9650 Rockville Pike, Bethesda MD 20814-3991. ISSN: 1931-857X, ESSN: 1522-1466. Visit our website at http://www.the-aps.org/.

Am J Physiol Renal Physiol 292: F723–F735, 2007.
First published October 24, 2006; doi:10.1152/ajprenal.00276.2006.

Acute growth hormone administration induces antidiuretic and antinatriuretic effects and increases phosphorylation of NKCC2

Henrik Dimke,[1] Allan Flyvbjerg,[2] Soline Bourgeois,[3] Klaus Thomsen,[4] Jørgen Frøkiær,[5] Pascal Houillier,[3] Søren Nielsen,[1] and Sebastian Frische[1]

[1]*The Water and Salt Research Centre, Institute of Anatomy, University of Aarhus, Aarhus;* [2]*Medical Department M and Medical Research Laboratories, Clinical Institute, Aarhus University Hospital, Aarhus;* [4]*Centre for Basic Psychiatric Research, Aarhus University Hospital;* [5]*The Water and Salt Research Centre, Clinical Institute, University of Aarhus, Aarhus, Denmark; and* [3]*Institut National de la Santé et de la Recherche Médicale U652, IFR58, Institut des Cordeliers, Université René Descartes and Université Pierre et Marie Curie, Paris, France*

Submitted 19 July 2006; accepted in final form 16 October 2006

Dimke H, Flyvbjerg A, Bourgeois S, Thomsen K, Frøkiær J, Houillier P, Nielsen S, Frische S. Acute growth hormone administration induces antidiuretic and antinatriuretic effects and increases phosphorylation of NKCC2. *Am J Physiol Renal Physiol* 292: F723–F735, 2007. First published October 24, 2006; doi:10.1152/ajprenal.00276.2006.—Growth hormone (GH) has antidiuretic and antinatriuretic effects in rats and humans, but the molecular mechanisms responsible for these effects are unknown. The aim of this study was to investigate the mechanisms behind the acute renal effects of GH in rats. Female rats received rat (r)GH (2.8 mg/kg sc) or saline and were placed in metabolic cages for 5 h. Urinary excretion of electrolytes and urinary volume were reduced after rGH injection, while urine osmolality was increased. Creatinine and lithium clearance remained unchanged, suggesting that rGH increases reabsorption in segments distal to the proximal tubule. Total plasma insulin-like growth factor I (IGF-I) levels did not change, while cortical IGF-I mRNA abundance was increased. The relative abundance of total and Ser^{256}-phosphorylated aquaporin 2 was found to be unchanged by immunoblotting, whereas a significant increase of Thr^{96} and Thr^{101}-phosphorylated NKCC2 (renal Na^+, K^+, $2Cl^-$ cotransporter) was found in the inner stripe of outer medulla thick ascending limbs (mTAL). Additionally, an increased NKCC2 expression was observed in the cortical region. Immunohistochemistry confirmed these findings. The density of NKCC2 molecules in the apical membrane of mTAL cells appeared to be unchanged after rGH injection evaluated by immunoelectron microscopy. Basolateral addition of rGH or IGF-I to microperfused rat mTAL segments did not change transepithelial voltage. In conclusion, GH appears to exert its acute antinatriuretic and antidiuretic effects through indirect activation of NKCC2 in the mTAL.

thick ascending limb; sodium; insulin-like growth factor I; GH; kidney

GROWTH HORMONE (GH) is secreted in a pulsatile pattern by the anterior pituitary (8) and has a number of well-known effects including stimulation of bone growth (28) and change in body composition (53). While disturbance of normal growth is a hallmark of abnormal GH secretion, these patients also present with a distorted sodium and water homeostasis. Hypersecretion of GH in acromegaly is associated with a larger extracellular volume (ECV) (27), and patients suffering from GH deficiency have a decreased ECV (52), which can be augmented by GH replacement therapy (4). Similarly, chronic administration of GH expands ECV (40) and decreases sodium excretion in healthy humans (21, 25, 31) and rats (63). The decrease in sodium excretion is often transient, only occurring within the initial period of GH administration (2, 3, 25, 31, 58).

Since sodium retention is only seen transiently in studies of chronic GH treatment, compensatory changes counteracting the antinatriuretic and antidiuretic effects of GH may be induced after a few days of GH treatment leading to a new steady state of sodium balance, albeit in some cases with expanded ECV. Moreover, GH-induced stimulation of other renotrophic hormones may also contribute to maintaining the expanded ECV. To understand the renal aspects of the complex state of chronic GH treatment, it is therefore necessary to dissect the changes in renal function into acute changes following shortly after a single GH injection and chronic (including compensatory) changes seen only upon repeated injections or similar chronic treatment.

In comparison to chronic GH administration, the initial (acute) effects of GH on renal water and sodium handling have been less studied. The available studies in humans report an acute decrease in urinary sodium excretion, within the first day of GH administration (2, 3). In rats, the acute antinatriuretic and antidiuretic effects of GH are more noticeable. Within few hours after a bolus injection of GH, a decrease in urinary volume and urinary electrolyte excretion is observed (32, 36, 54, 56). The pulsatile pattern of GH secretion in conjunction with the acute antinatriuretic and antidiuretic actions of the hormone suggests that GH is important, not only in pathophysiological states, but also as a component in the normal regulation of water and sodium balance, including a possible regulatory role in the circadian blood pressure rhythm (49).

The changes in renotrophic hormones seen in response to chronic GH administration have led to the investigation of these hormones as the prime mediators of the sodium- and water-retaining effects of GH. Chronic exposure to GH increases circulating and local insulin-like growth factor (IGF-I) production in healthy humans (21, 40, 41) and GH-deficient patients (4). However, the direct tubular actions of IGF-I are incompletely understood (23, 24). Several attempts to clarify the function of the renin-angiotesin-aldosterone (RAA) system in the antinatriuretic response observed after chronic GH ad-

Address for reprint requests and other correspondence: S. Frische, The Water and Salt Research Centre, Institute of Anatomy, Wilhelm Meyers Allé Bldg. 233/234, Univ. of Aarhus, 8000 Aarhus C, Denmark (e-mail: sfri@ana.au.dk).

The costs of publication of this article were defrayed in part by the payment of page charges. The article must therefore be hereby marked "*advertisement*" in accordance with 18 U.S.C. Section 1734 solely to indicate this fact.

ministration have also been made. However, the results are contradictory as some studies report an increased activity of one or more components of the RAA system, while other studies conclude differently (1, 21, 22, 25, 31, 41). Other hormones such as vasopressin (AVP) and atrial natriuretic factor have also been suspected to be involved in mediating the GH-induced antinatriuresis, but no changes were found in AVP concentrations (25, 40) and contradictory findings were observed regarding atrial natriuretic factor (21, 41). These studies were based on protocols of chronic GH exposure and thus do not address whether these hormones are involved in the primary effect of GH or in compensatory changes following prolonged GH treatment. Very few studies have investigated the acute effect of GH on renotrophic hormonal systems. In humans and rats, no change in plasma renin activity was seen after a bolus injection of GH (10, 26). Additionally, adrenalectomized rats receiving GH for 3 days show an immediate decrease in sodium excretion, in the same manner as normal rats (58). These studies indicate that the classical RAA system is not activated as part of the acute effect of GH.

To determine the mechanisms behind the acute effects of GH on electrolyte and water excretion, we decided to *1*) investigate the effects of rat GH (rGH) on renal reabsorption of sodium, potassium, chloride, and water in rats during the first 5 h after a single rGH injection, *2*) determine in which parts of the renal tubule rGH exerts its antinatriuretic and antidiuretic effects using lithium clearance, *3*) determine whether the circulating and renal concentrations of IGF-I were changed 5 h after a single rGH injection to assess whether the observed effects were due to a direct action of GH or indirectly through stimulation of IGF-I, *4*) investigate the molecular mechanisms behind the observed renal effects by determining the expression levels, phosphorylation levels (applying antibodies against the phosphorylated forms), and subcellular localization of the AVP-regulated water channel aquaporin 2 (AQP2) and the bumetanide-sensitive Na^+, K^+, Cl^--cotransporter (NKCC2) using immunoblotting, immunohistochemistry and immunoelectronmicroscopy, and *5*) determine whether the observed effects were directly mediated by rGH using the microperfused isolated tubuli system.

METHODS

Experimental animals. Animal experiments were performed following the Danish and French legislations on animal experiments and according to license number 2004/561–816 for use of experimental animals issued by the Danish Ministry of Justice and to licence number A75–06-10 for use of experimental animals issued by the Paris city Police Headquarters. Animals for experimental *protocols 1-3* were acquired from Taconic (M&B Ry, Denmark).

Experimental protocol 1. Twenty-four female Wistar-Hannover rats, weighing 190–210 g, were placed in metabolic cages 3 days before the experiment for acclimation. They were maintained on a standard rodent diet (Altromin 1321, Lage, Germany) with free access to food and water. On the day of the experiment, rats were divided randomly into two groups. One group ($n = 12$) received a bolus injection of rGH (2.8 mg/kg, Novo Nordisk, Gentofte, Denmark), diluted to a concentration of 1 mg rGH/ml saline. A control group ($n = 12$) was injected with an equal volume of physiological saline. Injections were given subcutaneously in the nape of the neck. Just before the injection, the rats were prompted to empty their bladders by being placed individually on a plate. Almost all of the rats voided spontaneously during these conditions (60). The rats were then weighed and placed in a clean metabolic cage. Five hours later, the rats were opened by a large laparotomy under halothane inhalation (3%, 5 l/min, Halocarbon laboratories). The bladder was emptied using a syringe and the content was pooled with the previously collected urine. The kidneys were either removed and dissected into zones [cortex/outer stripe of outer medulla (CTX/OSOM), inner stripe of outer medulla (ISOM), and inner medulla (IM)] for immunoblotting and real-time PCR, or the abdominal aorta was cannulated and the kidneys were perfusion fixed for immunohistochemical analysis. A blood sample was withdrawn from the vena cava for further analysis. Rats were killed with 10-min interval and injections were spaced accordingly. Water and food consumption and urine production during the 5-h protocol were measured. The experiment was repeated to obtain more blood for analysis and kidneys for immunoblotting and immunohistochemistry. However, during these repeats, the rats were not placed in metabolic cages and consequently no urine data were obtained.

Experimental protocol 2. To investigate whether the effects observed in *protocol 1* were due to changes in proximal tubular function, lithium clearance was used as an estimation of the proximal tubular sodium and water clearance. Twenty-four female Wistar-Hannover rats, weighing 200–220 g, were used in this experiment. Six days before the experiment, rats were placed in metabolic cages and maintained on a standard rodent diet, with an added sodium content of 200 mmol/kg dry fodder to prevent distal reabsorption of lithium. Three days before the experiment, the diet was supplemented with a low dose of lithium (12 mmol/kg dry food). Thirty minutes before the experiment started, blood was removed from the tail under isofluorane anaesthesia (3%, 5 l/min, Abbott Scandinavia AB), for analysis of Li^+ concentrations. The remainder of the experiment was carried out as experimental *protocol 1*; however, blood removed during the death was withdrawn from the abdominal aorta.

Experimental protocol 3. The study was carried out essentially as experimental *protocol 1*. However, one group of rats ($n = 6$) received a bolus injection of human (h)GH (2.8 mg/kg body wt; Norditropin, Novo Nordisk) diluted in saline, while control rats ($n = 6$) were injected with a placebo solution (Novo Nordisk) diluted in saline. Blood was removed for determination of hGH and rGH.

Measurements of solutes and creatinine. Total concentrations of sodium, potassium, and creatinine in plasma and urinary creatinine were determined using a Vitros 950 (Johnson and Johnson); total concentrations of sodium and potassium were determined by atomic absorption photometry (Eppendorf, FCM6341, Hamburg, Germany) by the department of Clinical Biochemistry, Clinical Institute, Aarhus University Hospital. Urinary and plasma concentrations of chloride (ABL 615, Radiometer, Copenhagen, Denmark) as well as the plasma and urine osmolality (Advanced Osmometer, model 3900, Advanced Instruments, Norwood, MA, and Osmomat 030-D, Gonotec, Berlin, Germany) were determined. The lithium concentration in plasma was measured using flame emission photometry. Urinary lithium concentration was measured by atomic absorption photometry.

Radioimmunoassays. Total plasma IGF-I levels were determined after acid-ethanol extraction as previously described (20). Intra- and interassay coefficients of variation (CVs) were <5 and 10%, respectively. Total plasma 22-kDa hGH was measured by a two-site fluoroimmunometric assay against two antigenic determinants on the 22-kDa hGH molecule with europium as the reporter molecule (Delfia, Wallac Oy, Turku, Finland). The level of detection is 0.03 mU/l. The intra- and interassay CVs at 0.5 mU/l were 5 and 8%, respectively (57). Plasma rGH was measured by RIA using a specific polyclonal rabbit rGH antibody and rGH as standard. The materials, including I^{125}-labeled rGH, were obtained from Amersham (Amersham International, Bucks, UK). Intra- and interassay CVs were <5 and <10%, respectively (20). Serum insulin was measured using a rat insulin ELISA Kit (DRG Diagnostics, Marburg, Germany), with intra- and interassay CVs <5 and 10%, respectively.

Real-time PCR. The method was performed as described previously (30). Briefly, total cellular RNA was extracted from kidney zones using 6100 Nucleic Acid PrepStation kit (Applied Biosystems). RNA was reverse transcribed using Multiscribe Reverse Transcriptase kit (Applied Biosystems). cDNA products were amplified by PCR by adding the cDNA to a *Taq* polymerase mixture (*Taq*Man Universal PCR MasterMix), with gene-specific primers against IGF-I (Rn00710306_m1) and the internal standard eukaryotic 18s rRNA (Hs99999901_s1) developed by Applied Biosystems. PCR products were detected by the cleavage of a *Taq*Man probe annealing to the product.

Primary antibodies. For semiquantitative immunoblotting, the following affinity-purified polyclonal antibodies were used. *1*) Rabbit polyclonal LL320 AP was a generous gift from Dr. M. Knepper (National Institutes of Health, Bethesda, MD) and has been extensively characterized earlier (34). *2*) Anti-p-NKCC2 9934 AP: this rabbit polyclonal antibody was raised against a phosphorylated epitope on NKCC2, earlier described in mice (16). The sequence stems from the NH_2 terminal of NKCC2 and corresponds to amino acids 91–106 in rat NKCC2 with threonine phosphorylations on Thr^{96} and Thr^{101}. The antibody was developed by immunizing a rabbit with the phosphorylated peptide ($YYLQT^{PO3}FGHNT^{PO3}MDAVP$). The antiserum was run through a column containing the corresponding nonphosphorylated peptide, plus an NH_2-terminal cysteine for conjugation (SulfoLink Antibody Immobilization kit, Pierce). The unbound fraction was then placed on a column containing the phosphorylated peptide, plus an NH_2-terminal cysteine (SulfoLink). The eluted fraction from the column containing immobilized phosphorylated peptide was used in this study. *3*) Anti-AQP2 (H7661 AP): this rabbit polyclonal antibody has been developed against the same epitope as the previously described LL127 (43). The sequence was derived from the COOH terminal of AQP2 (amino acids 250–271). The sequence was EVRRRQSVELHSPQSLPRGSKA (plus an NH_2-terminal cysteine used for conjugation during affinity purification). The antiserum was affinity purified against the immunizing peptide. The affinity-purified antibody recognized both the immunizing peptide, as well as a peptide including a phosphoserine at position 7, corresponding to serine 256 in rat AQP2. *4*) Phosphorylated-AQP2 (p-AQP2) (AN244-pp-AP): an affinity-purified rabbit polyclonal antibody to serine 256 phosphorylated AQP2 has previously been described (7). *5*) Calbindin (RDI-CALBINDabm): a monoclonal antibody against rat Calbindin was obtained from Research Diagnostics.

Preparation of tissue for semiquantitative immunoblotting. Kidney zones were placed in dissection buffer (0.3 M sucrose, 25 mM imidazole, 1 mM EDTA, pH 7.29), containing inhibitors against proteases and phosphatases (8.4 μM leupeptin, 4 mM pefablock, 100 nM okadaic acid, 25 nM sodium floride, and 1 mM sodium orthovanadate). The tissue was homogenized (Ultra turrax, T8 homogenizer, IKA labortechnik, Staufen, Germany) and centrifuged at 4,000 *g* for 15 min at 4°C (Beckman L8M). The samples were then solubilized in a SDS-containing sample buffer (final concentration in sample; 62.5 mM Tris, 3% SDS, 8.7% glycerol, 90 μM bromphenolblue, and 97.2 mM dithiothreitol) at 95°C for 10 min.

Electrophoresis and semiquantitative immunoblotting. Samples adjusted for protein concentration were run on 7.5–15% polyacrylamide minigels (Bio-Rad Mini Protean II) and transferred to nitrocellulose or PVDF membranes (Hybond-ECL or Hybond-P, Amersham Pharmacia Biotech, Little Chalfont, UK) by electroelution (0.025 M Tris, 0.19 M glycine, and 20% methanol, pH 8.3, 100 V, 1 h). The membranes were blocked using 5% skimmed milk in a PBS-T solution (80 mM Na_2PO_4, 20 mM NaH_2PO_4, 100 mM NaCl, 0.1% Tween 20, pH 7.5), washed, and incubated in primary antibody overnight at 4°C. The labeling was visualized using a horseradish peroxidase (HRP)-conjugated secondary antibody (P448, DAKO, Glostrup, Copenhagen, Denmark) and an enhanced chemiluminescence system (ECL) exposed to photographic film (Hyperfilm ECL). ECL films were scanned using an AGFA scanner (DUOSCAN f40). The densities of the bands were determined, using specific quantification software (Scion Image, Scion, Windows version of NIH-Image). Two-dimensional rolling ball background subtraction, and the Gel-plot2 macro, was used for the densitometric analysis.

Differential centrifugation. Kidney slices from the ISOM was homogenized and centrifuged at 1,000 *g* for 10 min. The supernatant was removed and pelleted at 4,000 *g* for 20 min. The pellet was rehomogenized and recentrifuged at 4,000 *g* for 20 min and subsequently resuspended in sample buffer. The 4,000-*g* supernatant was pelleted at 17,000 *g* for 30 min, rehomogenized, and recentrifuged at 17,000 *g* for 30 min and dissolved in sample buffer. The 17,000-*g* supernatant was spun at 200,000 *g* for 60 min. The resulting pellet was rehomogenized and recentrifuged at the respective speed and time and processed as above. The fractions, largely consisting of organelles and nuclei (4,000 *g*), plasma membranes (17,000 *g*), and vesicles (200,000 *g*) were processed for immunoblotting.

Preparation of tissue for light and laser microscopy. Kidneys were fixed by perfusion (3% paraformaldehyde in 0.1 M sodium cacodylate buffer, pH 7.4), removed, postfixated for 1 h, and dehydrated before being embedded in paraffin. Two-micrometer sections were cut from tissue blocks on a microtome (Leica Microsystems A/S, Herlev, Denmark).

Single labeling of tissue for light microscopy. Sections were dewaxed and rehydrated in a series of ethanol. During rehydration, endogenous peroxidase enzymes were blocked using 0.5% hydrogen peroxide (H_2O_2) in absolute methanol. To reveal antigens, sections were boiled in 10 mM Tris, 0.5 mM EGTA (pH 9.0), using a microwave oven. To block free aldehyde groups, the sections were placed in 50 mM NH_4Cl in PBS. The sections were then washed in a 0.01 M PBS solution (1% BSA, 0.2% gelatine, and 0.05% saponin) and incubated overnight at 4°C with primary antibody (0.1% BSA, 0.3% Triton X-100 in PBS). Sections were rinsed in a PBS solution (0.1% BSA, 0.2% gelatine, 0.05% saponin) and incubated in a secondary antibody solution (0.1% BSA, 0.3% Triton X-100 in PBS) containing HRP-conjugated secondary antibodies (P448, DAKO). Antibody binding was visualized using 3,3′-diaminobenzidine (Kem-En-Tec, Copenhagen, Denmark) in 0.003% H_2O_2. Sections were counterstained with Mayer's hematoxylin, dehydrated, and mounted using Eukitt reagent (Eukitt, O. Kindler GmbH and Company). Light microscopy was carried out using a Leica DMRE light microscope (Leica Microsystems A/S).

Double labeling of tissue for laser confocal microscopy. Sections were processed as above, except endogenous peroxidases were not blocked and monoclonal (Calbindin) and polyclonal antibodies (p-NKCC2 AP) were incubated together overnight. Visualization was achieved using goat-anti-rabbit and goat-anti-mouse flurophore-conjugated secondary antibodies (Alexa488 anti-rabbit, Alexa546 anti-mouse, highly cross adsorbed, Molecular Probes). Double labeling was also performed using two polyclonal antibodies (p-NKCC2 and NKCC2). After incubation with the NKCC2 antibody and the Alexa546-conjugated secondary goat anti-rabbit antibody, rabbit IgG cross-binding was blocked using 10% rabbit serum (dissolved in 0.1% BSA, 0.3% Triton X-100 in PBS) and endogenous biotin was blocked using a commercial biotin blocking kit (product no. X0590, DAKO). Then a second labeling was performed using a primary rabbit antibody (p-NKCC2) conjugated to biotin (EZ-Link Sulfo-NHS-LC-Biotin, product no. 21335, Pierce, Rockford, IL) and secondary Fluoresein (FITC)-conjugated streptavidin. The microscopy was carried out using a Leica DMIRE2 laser confocal microscope (Leica Microsystems A/S).

Immunoelectronmicroscopy. Tissue blocks were infiltrated with 2.3 M sucrose, mounted on metal holders, and rapidly frozen in liquid nitrogen. Frozen tissue blocks were subjected to cryosubstitution and Lowicryl HM20 embedding. Cryosubstitution was performed as previously described (38). Ultrathin (45 nm) Lowicryl sections were cut on a ultramicrotome (Reichert Ultracut S), preincubated with 0.05 M Tris, 0.1% Triton X-100 (pH 7.4) containing 0.1% sodium borohy-

dride, and 0.05 M glycine followed by incubation with 0.05 M Tris, 0.1% Triton X-100 (pH 7.4) containing 0.2% skimmed milk. The preincubation was followed by incubation with affinity-purified antibodies against rat NKCC2 and phosphorylated-NKCC2. Labeling was visualized with goat anti-rabbit IgG conjugated to 10-nm colloidal gold particles. Grids were stained with uranyl acetate for 10 min and with lead citrate for 18 s. Pictures were obtained using a Megaview III CCD camera (Soft Imaging System). Analysis of NKCC2 membrane density was done manually by counting gold particles in the membrane (within an area of ~30 nm on each side of the membrane) and dividing it by the length of the membrane studied, which was measured using an opisometer.

Microperfusion of isolated mTAL segments. Pathogen-free female Wistar rats weighing 60–75 g (Charles River Laboratories) were allowed free access to autoclaved standard rat chow and distilled water until the time of experiments. Rats were anesthetized with 50 mg/kg ip pentobarbital sodium 10 min after injection of 2 mg furosemide ip to limit medullary thick ascending limb (mTAL) oxygen consumption during the time of tubule dissection. Both kidneys were cooled in situ with control bath solution for 1 min and then removed and cut into thin coronal slices for tubule dissection. These maneuvers have been shown to improve the viability of renal tubules in vitro (14, 19). Noteworthy, in vivo intraperitoneal furosemide injection does not prevent the ability of NaCl transport in the mTAL to be subsequently stimulated in vitro by 10^{-9} M AVP (P. Houillier, unpublished results). The mTAL segments were dissected from the ISOM at 4°C in the control bath solution of the experiment. The isolated tubule was transferred to the bath chamber on the stage of an inverted microscope (Axiovert 100, Carl Zeiss, Germany) and mounted on concentric glass pipettes for microperfusion at 37°C. The length of the perfused segments ranged from 0.45 to 0.8 mm. The perfusion (lumen) and bath solutions contained 142 mM Na, 4 mM K, 2 mM Ca, 1.2 mM Mg, 118 mM Cl, 23 mM HCO_3, 2 mM lactate, 5 mM HEPES, 1.2 mM SO_4, 1 mM citrate, 2 mM HPO_4, 5 mM glucose, and 5 mM alanine. The osmolarity of the solution was 295 ± 5 mosM. All solutions were equilibrated with 95% O_2-5% CO_2. pH ranged from 7.38 and 7.43 at 37°C. The bath solution also contained 0.2% fraction V bovine serum albumin. Transepithelial voltage (V_{te}) was measured with a DP-301 differential electrometer (Warner Instrument, Hamden, CT) by the use of a Ag/AgCl electrode connected to the perfusion pipette via a 0.15 M NaCl agar bridge; a 0.15 M NaCl agar bridge also connected the peritubular bath to a Ag/AgCl electrode. V_{te} was measured during each period at the tip of the perfusion pipette.

Study protocol. The tubules were equilibrated for 20–30 min at 37°C in the initial perfusion and bath solutions and the luminal flow was adjusted to 10 nl/min. Three periods were successively performed on each tubule: initial, experimental, and recovery; after initial recording of V_{te}, the tubules were exposed to rGH or IGF-I in the bath, V_{te} was recorded again and finally V_{te} was recorded in the absence of the hormones. The dose of rGH was chosen based on the results of experimental *protocol 3* to match the expected plasma concentration of rGH in experimental *protocol 1*. Five hours after hGH injection in experimental *protocol 3*, plasma concentration amounted to $8.07 \times 10^{-9} \pm 2.58 \times 10^{-9}$ M hGH ($n = 6$), while plasma concentrations of rGH averaged $2.95 \times 10^{-10} \pm 1.5 \times 10^{-10}$ M rGH ($n = 6$). Therefore, a concentration of 10^{-8} M of rGH was added basolaterally in these experiments. IGF-I was used at 5×10^{-8} M, a dose earlier used in proximal tubules by Quigley and Baum (50).

Calculations of lithium clearance. Renal clearances (C) and fractional excretions (FE) were calculated by the standard formulas as follows: $C = U \times V/P$; $FE = C/GFR$, where U is urine concentration, V is the urine flow rate, P is the plasma concentration, and GFR is the glomerular filtration rate as measured by creatinine clearance. Lithium clearance (C_{Li}) was calculated as $C_{Li} = V \times U_{Li}/P_{Li}$, where $P_{Li} = (P_{Li}, \text{before} + P_{Li}, \text{after})/2$. Fractional Li^+ excretion was calculated as C_{Li}/CCr, distal fractional Na^+ excretion as CNa/C_{Li}, and distal fractional water exretion as V/C_{Li}. C_{Li} was used as an index of the proximal tubular fluid output, and the fractional Li^+ exretion was used as an index of the fractional delivery of sodium and fluid from the proximal tubules (58, 60).

Statistical analysis. Values are presented as means ± SD and presented as control vs. GH injected. Comparisons between two groups were made using an unpaired *t*-test ($P < 0.05$ is considered statistically significant).

RESULTS

rGH increases reabsorption of electrolytes and water in segments distal to the proximal tubule. A bolus injection of rGH significantly reduced urinary volume ($P < 0.001$) and raised urinary osmolality ($P < 0.005$) in experimental *protocol 1* (Table 1). No differences in food ($P = 0.82$) and water ($P = 0.18$) intake were observed during the 5-h period. Still, administration of rGH resulted in a significant reduction in the urinary excretion of sodium ($P < 0.0001$), potassium ($P < 0.003$), and chloride ($P < 0.0002$; Table 1). The creatinine clearance

Table 1. *Renal function in saline and rGH-injected rats*

	CON	rGH
Experimental *protocol 1*		
Food intake, g·kg^{-1}·5 h^{-1}	6.1±4.3 (*n*=12)	6.4±3.8 (*n*=12)
Water intake, ml·kg^{-1}·5 h^{-1}	24.8±9.3 (*n*=12)	32.0±15.9 (*n*=12)
Urinary output, μl·min^{-1}·kg^{-1}	55.3±20.3 (*n*=12)	30.8±11.1 (*n*=12)*
Sodium excretion, μmol·min^{-1}·kg^{-1}	5.65±1.85 (*n*=12)	2.54±1.23 (*n*=11)*
Potassium excretion, μmol·min^{-1}·kg^{-1}	9.50±2.04 (*n*=12)	6.59±2.17 (*n*=11)*
Chloride excretion, μmol·min^{-1}·kg^{-1}	9.61±2.65 (*n*=12)	5.51±1.74 (*n*=12)*
Creatinine clearance, ml·min^{-1}·kg^{-1}	3.81±0.75 (*n*=12)	3.77±1.09 (*n*=11)
Fractional water excretion, %	1.44±0.38 (*n*=11)	0.88±0.37 (*n*=11)*
Fractional Na^+ excretion, %	1.08±0.24 (*n*=12)	0.49±0.22 (*n*=10)*
Fractional K^+ excretion, %	66±11 (*n*=12)	46±13 (*n*=10)*
Fractional Cl^- excretion, %	2.7±0.50 (*n*=10)	1.5±0.47 (*n*=10)*
Urine osmolality, mosmol/kgH_2O	1,106±207 (*n*=12)	1,509±394 (*n*=12)*
Experimental *protocol 2*		
Fractional Li^+ excretion, %	30.1±13.5 (*n*=11)	30.5±9.6 (*n*=9)
Distal fractional Na^+ excretion, %	2.43±0.73 (*n*=11)	0.90±0.42 (*n*=9)*
Distal fractional water excretion, %	2.38±0.84 (*n*=11)	1.37±0.30 (*n*=10)*

Values are presented as means ± SD and *n* represents the number of rats. *$P < 0.05$ is considered statistically significant.

Table 2. *Circulating IGF-I, renal IGF-I mRNA expression, and circulating insulin in saline- and rGH-injected rats*

	CON	rGH
Total IGF-I, μg/l	655±32.9 (n=9)	686±85.9 (n=10)
Insulin, μg/l	1.09±0.30 (n=6)	1.07±0.25 (n=6)
Renal IGF-I mRNA (fraction of control)		
CTX/OSOM	1.00±0.34 (n=6)	2.04±0.88 (n=6)*
ISOM	1.00±0.23 (n=6)	1.16±0.12 (n=6)
IM	1.00±0.19 (n=6)	1.20±0.61 (n=6)

Values are presented as means ± SD and n represents the number of rats. *$P < 0.05$ is considered statistically significant.

(estimate of GFR; $P = 0.91$) did not diverge between the groups (Table 1) and consequently a significant decrease in the fractional excretion of sodium ($P < 0.00001$), potassium ($P < 0.0009$), chloride ($P < 0.00003$), and water ($P < 0.001$) was observed in the rGH-injected group (Table 1). To investigate whether rGH increases sodium and water reabsorption in the proximal tubule, an analogous experiment was performed (experimental *protocol 2*). In this experiment, dietary sodium was increased to 200 mmol/kg dry food, and rats received a low dose of lithium for 3 days. The experiment returned essentially the same results as experimental *protocol 1*, i.e., a reduction in the fractional excretion of electrolytes and urinary volume (data not shown). The fractional excretion of lithium did not vary between the rGH- and saline-injected groups ($P = 0.95$). Thus no difference in the estimated fractional excretion of sodium and water in the proximal tubule occurs within the 5 h after rGH injection. The estimated fractional excretion of sodium ($P < 0.00003$) and water ($P < 0.002$) in segments distal to the proximal tubule was significantly decreased after injection of rGH (Table 1).

Changes in circulating and renal IGF-I after rGH injection. Both circulating and renal production of IGF-I are increased after chronic GH administration in rats (5, 39). However, little is known about the dose and time dependency of this response. In a suspension of collecting ducts IGF-I production occurs after 2 h of GH incubation in vitro (51), but the acute in vivo response to GH remains largely unknown. Since acute IGF-I administration induces antinatriuretic and antikaliuretic effects (17, 24), circulating and renal production of IGF-I was determined 5 h after injection of rGH. No difference in plasma concentrations of total IGF-I was observed between the saline-injected and rGH-injected group ($P = 0.31$; Table 2). To investigate whether renal IGF-I production was increased 5 h after injection of rGH, semiquantitative real-time PCR was performed on cDNA isolates from renal zones. A significant increase in IGF-I mRNA abundance was observed in the CTX/OSOM ($P < 0.02$), while the ISOM ($P = 0.16$) and IM ($P = 0.47$) showed no change in IGF-I mRNA content (Table 2). Increases in insulin are often observed after GH treatment, since GH decreases insulin sensitivity (37). As insulin has direct effects on renal transport mechanisms in rats (11, 29), insulin levels were measured 5 h after rGH injection. No change in serum insulin concentration was observed between the groups ($P = 0.90$; Table 2).

Phosphorylation level and subcellular localization of AQP2 remains unaffected after rGH administration. To investigate whether the antidiuretic effect of rGH was associated with increased phosphorylation and subcellular rearrangement of AQP2, semiquantitative immunoblotting and immunohistochemistry were used. Immunoblots and immunohistochemistry using anti-phosphorylated-AQP2 (p-AQP2) antibody, selectively recognizing phosphorylated serine 256, revealed no difference in the phosphorylation level of AQP2 between rats injected with rGH or saline (Fig. 1, *A*-*B*). Moreover, no change in the total amount of AQP2 was observed in any of the

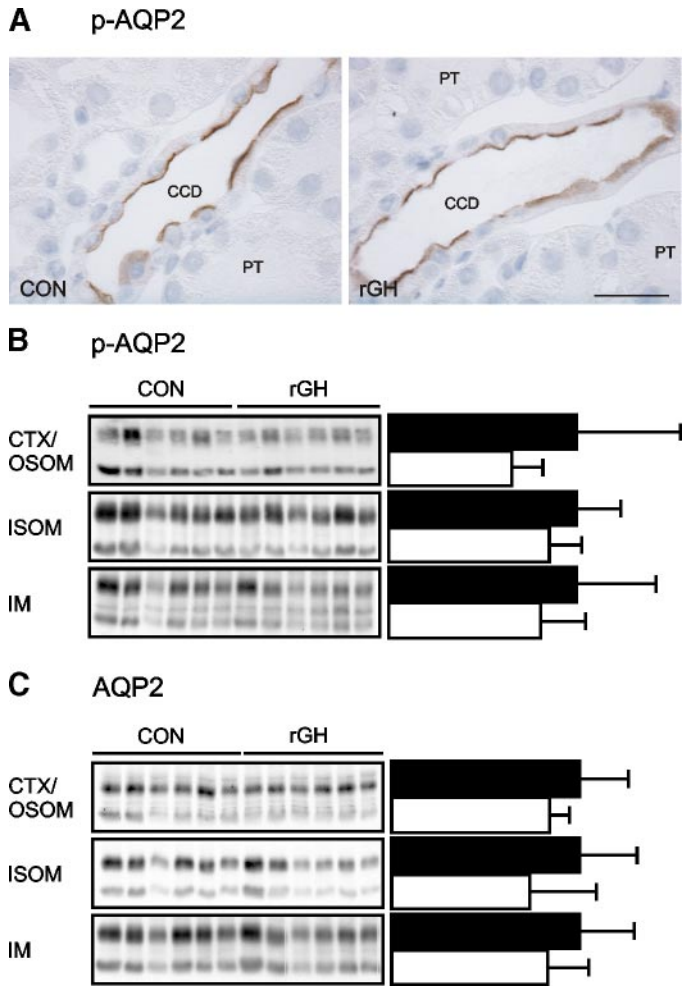

Fig. 1. Analysis of aquaporin-2 (AQP2) localization, abundance, and phosphorylation level. *A*: immunolabelings of Ser^{256} phosphorylated-AQP2 (p-AQP2) on 2-μm kidney sections from saline- and rat growth hormone (rGH)-injected rats. Pictures were obtained through a ×63 objective. Scale bar = 25 μm. PT, proximal tubule; CCD, cortical collecting duct. *B*: semiquantitative immunoblots of proteins from the cortex/outer stripe of outer medulla (CTX/OSOM), inner stripe of outer medulla (ISOM), and inner medulla (IM) incubated with anti-p-AQP2 antibodies. The graphs represent p-AQP2 abundance in rGH-injected (open bars) rats as a fraction of the abundance in saline-injected rats (filled bars). The values are CTX/OSOM: 1.0 ± 0.51 vs. 0.64 ± 0.15, $P = 0.15$; ISOM: 1.0 ± 0.23 vs. 0.85 ± 0.17, $P = 0.24$; and IM: 1.0 ± 0.42 vs. 0.80 ± 0.24, $P = 0.34$. *C*: semiquantitative immunoblots of proteins from the CTX/OSOM, ISOM, and IM incubated with anti-AQP2 antibodies. The graphs represent AQP2 protein abundance in rGH-injected (open bars) rats as a fraction of the abundance in saline-injected rats (filled bars). The values are CTX/OSOM: 1.0 ± 0.25 vs. 0.83 ± 0.10, $P = 0.17$; ISOM: 1.0 ± 0.30 vs. 0.73 ± 0.35, $P = 0.19$; and IM: 1.0 ± 0.29 vs. 0.82 ± 0.22, $P = 0.26$. Data are expressed as means ± SD and represent $n = 6$ for each group. The 2 bands with an approximate molecular weight of 28 and 35–50 kDa correspond to the nonglycosylated and glycosylated form of AQP2, respectively. Both were used for densitometric analyses.

segments investigated (Fig. 1*C*), and no subcellular shift was observed in the phosphorylated fraction of AQP2 (Fig. 1*A*) nor in the total amount of AQP2 in the segments investigated (data not shown).

Characterization of an anti-phosphorylated-NKCC2 antibody. Since the antidiuretic effect and the increased urinary osmolality observed in rats injected with rGH appeared to be independent of increased collecting duct water permeability, we decided to investigate the possibility that rGH could augment the osmotic driving force between the collecting duct lumen and the interstitium. As NKCC2 is a key player in the establishment of the osmotic gradient, the possibility that NKCC2 was regulated in response to rGH administration was investigated using an antibody specific to the Thr^{96} and Thr^{101}-phosphorylated NKCC2. Phosphorylation at these sites has been shown to be necessary for increasing the maximal transport activity of NKCC2 (15). To validate that the anti-phosphorylated-NKCC2 (p-NKCC2) antibody recognizes the phosphorylated epitope in NKCC2, peptide recognition and peptide preabsorption were evaluated. The affinity-purified anti-p-NKCC2 antibody selectively recognized the phosphorylated peptide, but not the nonphosphorylated peptide on immunoblots (Fig. 2*A*). When homogenates from kidney ISOM were subjected to differential centrifugation, SDS-PAGE, and immunoblotting, the anti-p-NKCC2 antibody produced a band between 150 and 250 kDa in the 4,000- and 17,000-*g* pellets, but not in the 200,000-*g* pellet (Fig. 2*B*). Thus, the anti-p-NKCC2 antibody recognizes a band with a molecular weight matching that reported for NKCC2 (34) and associates predominantly with the plasma membrane fraction. The localization of the phosphorylated form of NKCC2 was determined on immunohistochemical sections, using the anti-p-NKCC2 antibody. Staining was confined to the apical domains of the epithelial cells in the TAL, where the phosphorylated form of NKCC2 earlier has been found in mice (16) and in apical domains of the macula densa (MD) cells (Fig. 3*A*). In addition to the staining observed in the TAL/MD cells, the anti-p-NKCC2 antibody revealed weak staining in the distal convoluted tubules. The staining was confined to very apical domains of the DCT cells, where a narrow rim of labeling was evident (Fig. 3*A*). On immunohistochemical sections, preabsorption of the anti-p-NKCC2 antibody with the nonphosphorylated peptide did not remove any significant amount of staining (Fig. 3*B*), whereas all staining was completely inhibited, when the antibody was preabsorbed with the phosphorylated peptide (Fig. 3*C*). Double labeling with anti-calbindin and anti-p-NKCC2 confirmed that an anti-p-NKCC2 signal was present in calbindin-positive cells (Fig. 3, *D-F*). Double labeling with anti-NKCC2 and anti-p-NKCC2 (biotin conjugated) confirmed the absence of NKCC2 signal in a fraction of the p-NKCC2-positive cells (Fig. 3, *G-H*). We therefore conclude that the anti-p-NKCC2 antibody selectively recognizes the phosphorylated epitope on NKCC2. Moreover, the immunohistochemical labeling of the DCT indicates that the antibody also recognizes the sodium chloride cotransporter (NCC), which is also known to be phosphorylated on a homologous epitope (42). Since this epitope is also conserved in NKCC1 (the secretory Na^+, K^+, $2Cl^-$ cotransporter), we investigated whether the antibody has affinity for the phosphorylated form of NKCC1 in the parotid gland (12). Indeed, the antibody labeled basolateral domains in these cells (Fig. 3*I*), supporting that the antibody is specific against the Thr^{96} and Thr^{101}-phosphorylated form of NKCC2, and corresponding phosphorylated epitopes in NKCC1 and NCC in rats. Based on immunohistochemistry, the anti-p-NKCC2 antibody appears to recognize similar epitopes in mice and humans (data not shown).

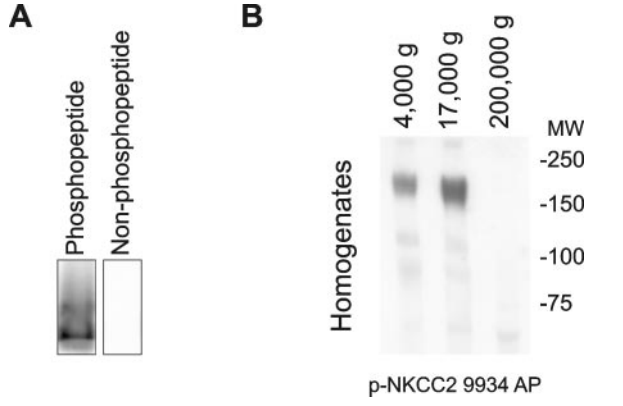

Fig. 2. Characterization of the anti-p-NKCC2 antibody using immunoblotting. *A*: immunoblots of phospho and nonphospho peptides derived from the NKCC2 sequence using the anti-p-NKCC2 antibody. *B*: anti-p-NKCC2 immunoblots of rat ISOM homogenates subjected to differential centrifugation: 4,000-*g* centrifugation pellet consists of larger cellular organelles, 17,000-*g* centrifugation pellet consists largely of plasma membrane vesicles, and 200,000-*g* centrifugation pellet consists largely of intracellular vesicles.

Phosphorylated form of NKCC2 is localized exclusively in the apical plasma membrane. Immunogold electron microscopy was used to investigate the subcellular localization of p-NKCC2 and NKCC2. The anti-NKCC2 antibody labeled apical membrane domains and intracellular domains in MD, cortical TAL (cTAL), and mTAL (Fig. 4, *A-C*). In contrast, incubation of kidney sections with the anti-p-NKCC2 antibody showed immunogold labeling almost exclusively in or below 100 nm from the apical plasma membrane (Fig. 4, *D-F*). It was not possible to investigate the labeling of the anti-p-NKCC2 antibody in the DCT, probably due to a lower affinity of the antibody for the NCC-epitope or poor conservation of this epitope in Lowicryl embedding.

Increased phosphorylation of NKCC2 in rGH-treated rats. Semiquantitative immunoblotting using the anti-NKCC2 antibody and anti-p-NKCC2 antibodies showed a significant increase in the abundance of phosphorylated NKCC2 and in the total abundance of NKCC2 protein in samples from the CTX/OSOM (Fig. 5*A*). In the ISOM, a significant increase in the abundance of phosphorylated NKCC2 was observed in rats injected with rGH (Fig. 5*B*), whereas no difference in the total amount of NKCC2 protein was observed (Fig. 5*B*). To estimate the degree of phosphorylation of NKCC2, the density measured using anti-p-NKCC2 was normalized to the density measured using anti-NKCC2 on immunoblots by first probing immunoblots with the anti-p-NKCC2 antibody, stripping them in glycine buffer (pH < 3), and reprobing them with anti-NKCC2-antibody. In the CTX/OSOM, a 1.03-fold increase in the degree of NKCC2 phosphorylation was found ($P = 0.80$) when normalized to the total amount of NKCC2 in the sample (Fig. 5*A*). In the ISOM, a 2.42-fold increase was observed in the rGH-treated group ($P < 0.03$), when normalized to the total amount of NKCC2 in the sample (Fig. 5*B*).

To confirm that phosphorylation was increased in the kidney of rGH-injected rats, sections of paraffin-embedded rat kidneys

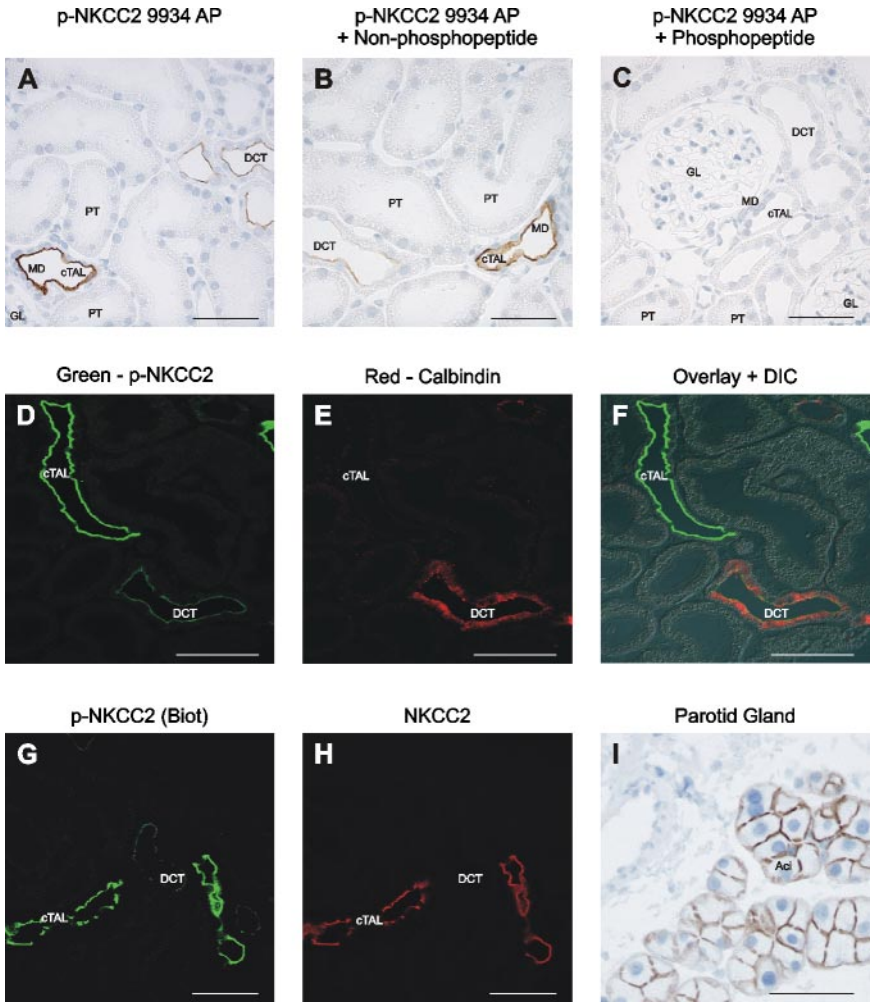

Fig. 3. Characterization of the anti-p-NKCC2 antibody using immunohistochemistry. *A-C*: immunolabelings on 2-μm rat kidney sections using the p-NKCC2 antibody (*A*), preabsorbed with nonphosphopeptide (*B*), or phosphopeptide (*C*). Pictures from the CTX were obtained through a ×25 objective, scale bars = 50 μm. Note weak labeling in the distal convoluted tubule (DCT). *D-F*: confocal laser microscopy of double-labeled rat kidney sections using polyclonal anti-p-NKCC2 (*D*), monoclonal anti-calbindin (*E*), and overlay (*F*). Pictures were obtained through a ×63 objective, scale bars = 25 μm. *G-H*: confocal laser microscopy of double-labeled rat kidney sections using anti-p-NKCC2 conjugated to biotin (*G*) and anti-NKCC2 (*H*). *I*: anti-p-NKCC2 immunolabeling of rat parotid gland. Pictures were obtained through a ×25 objective, scale bar = 50 μm. G, glomerulus; cTAL, cortical thick ascending limb; MD, macula densa; Aci, acinus cell.

labeled with the anti-p-NKCC2 antibody were studied. In the CTX and OSOM, no systematic difference in intensity of labeling was observed between kidney sections from rGH-injected and saline-injected rats (Fig. 6, *A-B*). In contrast, a marked increase in anti-p-NKCC2 staining was seen in the TAL of the ISOM of rGH-injected rats compared with controls (Fig. 6, *C-D*). Note that in saline-injected rats, staining in the cortical region is more intense than in the ISOM (Fig. 6, *A* and *C*). This axial heterogeneity has also been reported earlier in mice (16).

No change in the density of NKCC2 in the membrane of mTAL cells in the ISOM. Using light microscopy, no change in the subcellular localization of NKCC2 in the CTX, OSOM, and ISOM was seen 5 h after rGH injection. Since it has been shown that phosphorylation and apical targeting of NKCC2 increase in response to vasopressin (16), immunogold electron microscopy was employed using the anti-NKCC2 antibody to investigate whether a more subtle shift in NKCC2 was observed in mTAL cells (Fig. 7). In three saline and three rGH-injected rats, six cross sections of mTAL tubuli (ISOM) were counted (~60 pictures per animal). No difference in the density of NKCC2 in the membrane was observed (4.3 ± 0.47 vs. 5.0 ± 0.74 gold particles/μm membrane, $P = 0.23$) between rats injected with rGH or saline (Fig. 7).

rGH does not change V_{te} in isolated perfused mTAL. To evaluate whether rGH directly increases NKCC2 activity, V_{te} was measured in isolated microperfused mTAL (ISOM) nephron segments. Peritubular addition of rGH (10^{-8} M) did not change V_{te} (control 6.2 ± 2.8 mV, rGH 5.8 ± 1.8 mV, recovery 5.5 ± 1.6 mV, $n = 5$; Fig. 8*A*), suggesting that the effect of rGH is not direct. Therefore, it was investigated whether peritubular addition of IGF-I (5×10^{-8} M) had an effect on V_{te}. Again, no change in V_{te} was observed after peritubular addition of IGF-I (control 7.5 ± 3.7 mV, IGF-I 7.4 ± 2.6 mV, recovery 6.8 ± 2.7 mV, $n = 4$; Fig. 8*B*). In both sets of experiments, AVP (10^{-10} M) was used as a positive control in some of the tubules. Peritubular addition of AVP induced a mean increase in V_{te} by 2.47 ± 0.98 mV ($P < 0.05$; Fig. 8*C*).

DISCUSSION

The results of the present study strongly suggest that the antinatriuretic effect of GH is mediated by an increased phosphorylation level of NKCC2 in the mTAL of the ISOM and by increasing expression of NKCC2 in the cTAL, which leads to increased NaCl reabsorption by the TAL. This single effect could account for the antidiuretic effect of GH, by increasing the osmotic driving force for water reabsorption from the thin descending limbs of the loop of Henle and the collecting ducts.

In response to acute administration of rGH, a decrease in the urinary excretion of sodium, potassium, and chloride, and a

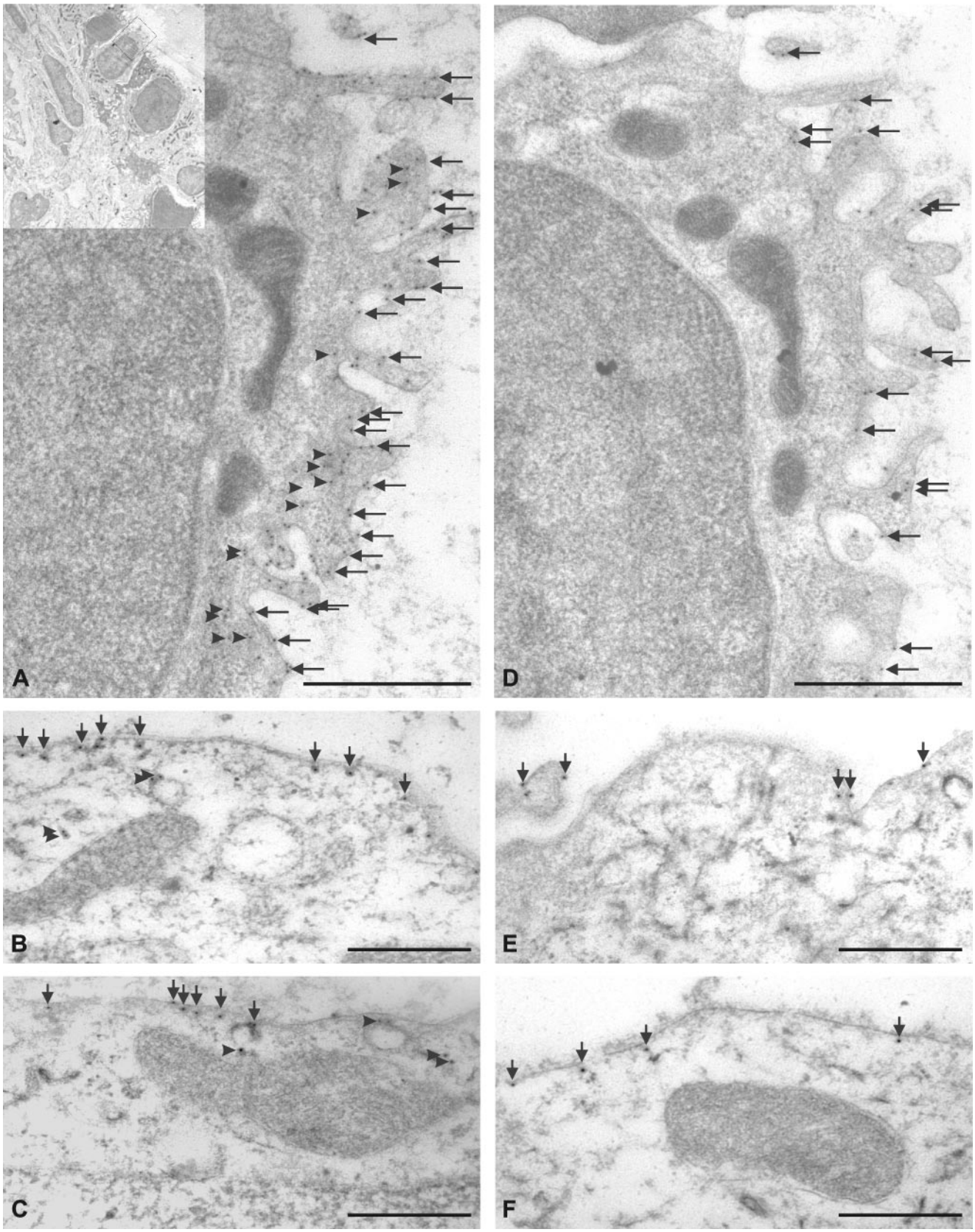

Fig. 4. Immunoelectron microscopy of cross-sections from macula densa (MD; *A*, *D*) and thick ascending limb (TAL) cells in the cortex (*B*, *E*) and ISOM (*C*, *F*). Labeling was visualized with 10-nm gold particles conjugated to antibodies against rabbit IgG. *A-C*: anti-NKCC2 antibody was associated with intracellular vesicles (arrowheads) and the apical plasma membrane (arrows) of MD and TAL cells. *D-F*: labeling with the anti-p-NKCC2 antibody was almost exclusively associated with the apical plasma membrane (arrows). Scale bars = 500 nm.

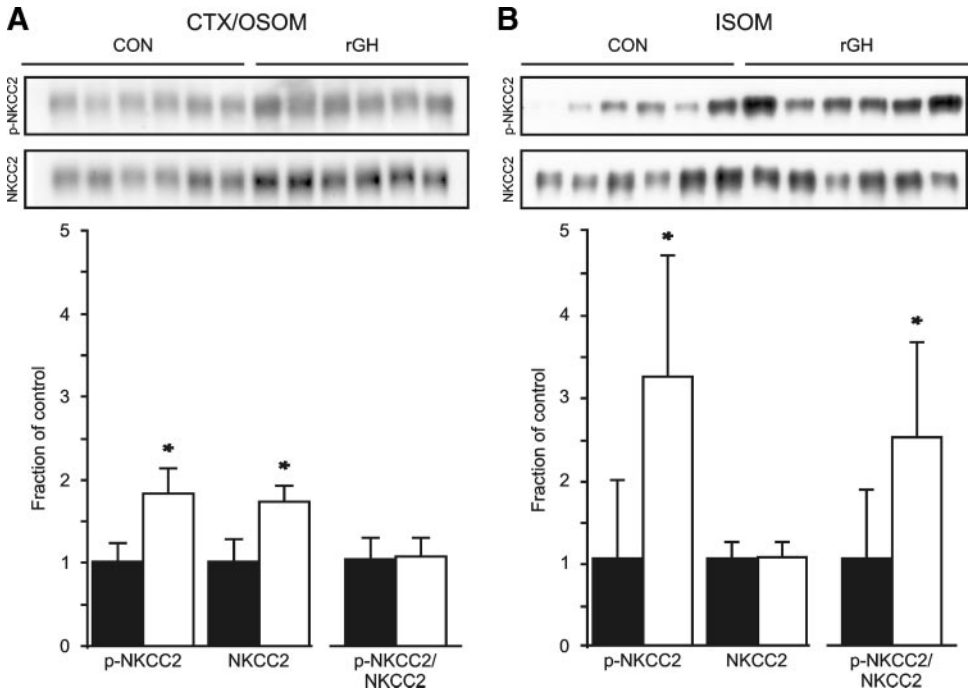

Fig. 5. Semiquantitative immunoblotting of proteins using polyclonal anti-p-NKCC2 and anti-NKCC2 antibodies. *A*: phosphorylation levels and total expression of NKCC2 in isolates from the CTX/OSOM of saline- (filled bars) and rGH-injected (open bars) rats. Graphs represent the average of the band densities from rGH-injected group as fractions of the average of the control group. p-NKCC2: 1.0 ± 0.23 vs. 1.8 ± 0.30, $P < 0.0003$; NKCC2: 1.0 ± 0.27 vs. 1.7 ± 0.19, $P < 0.0003$. The p-NKCC2/NKCC2 ratio is also depicted on the graph (1.00 ± 0.25 vs. 1.03 ± 0.21, $P = 0.80$). *B*: phosphorylation levels and total expression of NKCC2 in protein isolates from the ISOM. p-NKCC2: 1.0 ± 0.91 vs. 3.1 ± 1.41, $P < 0.02$; NKCC2: 1.0 ± 0.20 vs. 1.0 ± 0.17, $P = 0.83$; p-NKCC2/NKCC2: 1.0 ± 0.80 vs. 2.4 ± 1.10, $P = 0.03$. Data are expressed as means ± SD and represent $n = 6$ for each group. *$P < 0.05$ is considered statistically significant.

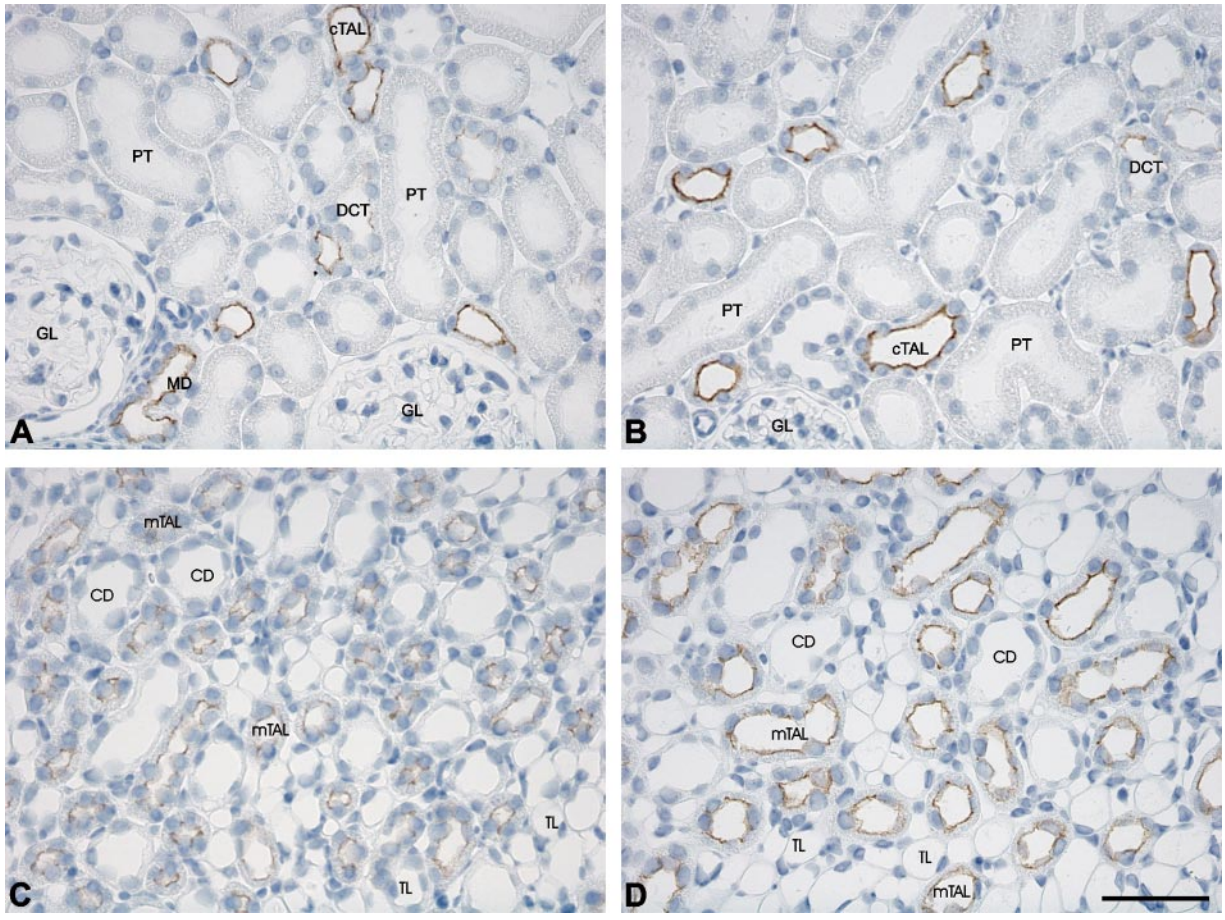

Fig. 6. Immunolabelings of p-NKCC2 in 2-μm sections from kidneys of saline (*A*, *C*)- and rGH-injected rats (*B*, *D*). *A-B*: labeling with the anti-p-NKCC2 antibody in the CTX. *C-D*: labeling with the anti-p-NKCC2 antibody in the ISOM. A marked increase in p-NKCC2 immunostaining is observed in the ISOM of rats injected with rGH. Pictures were obtained through a ×25 objective. Scale bar = 50 μm.

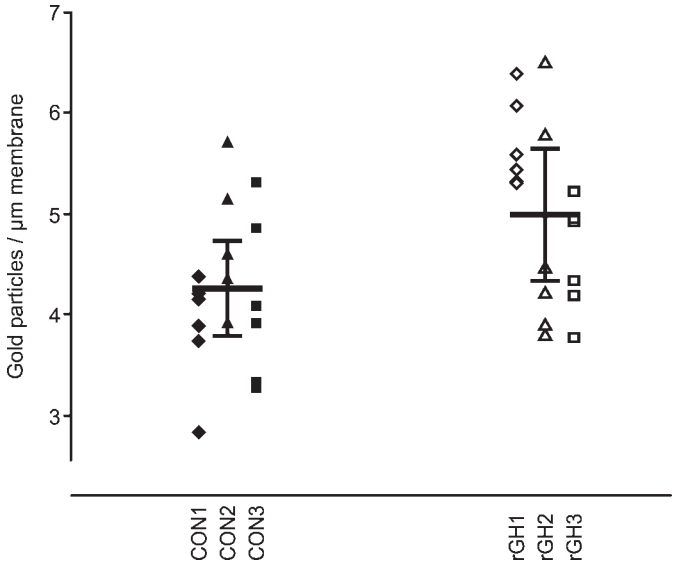

Fig. 7. Immunogold electron microscopy using the anti-NKCC2 antibody was employed to investigate the density of immunogold-labeled NKCC2 transporters in the apical membrane of medullary TAL (mTAL) cells (ISOM). Horizontal bars in the graph denote the group average, determined as gold particles per membrane length per animal (n = 3). Each data point in the figure represents the average number of gold particles per micrometer apical membrane in a single tubular cross section.

decrease in urinary volume were observed in experimental *protocol 1* and *2*. These findings are in accordance with earlier studies using hGH in rats (32, 54, 56). Since rGH administration did not increase GFR, it can be concluded that the electrolyte and water retention is due to increased tubular reabsorption. This is also evident from the observed decreases in the fractional excretions of electrolytes and water. In addition, an increase in urine osmolality was observed.

Two previous studies have investigated the clearance of lithium during GH treatment (21, 31). However, both experiments employed a protocol of chronic GH administration and investigated the clearance of lithium after at least 5 days of GH injections. In this experiment, focus was placed on finding where in the renal tubule rGH exerted its acute antinatriuretic and antidiuretic effect. The results from experimental *protocol 2* show no difference in the fractional excretion of lithium. Thus the estimated fractional excretion of sodium and water from the proximal tubule remains unchanged after rGH injection. This suggests that the acute antidiuretic and antinatriuretic effects observed after acute rGH administration occur in segments distal to the proximal tubule. This is supported by a previous study, where volume absorption was unchanged in perfused rabbit proximal convoluted tubules, after addition of GH (50).

Phosphorylation sites have been described in the NKCC2, the NKCC1, and the NCC cotransporters corresponding to Thr^{96}, Thr^{101}, and Thr^{114} in rat NKCC2, Thr^{203}, Thr^{208}, and Thr^{221} in rat NKCC1 and, Thr^{53}, Thr^{58}, Ser^{71} in rat NCC (12, 16, 42). The anti-p-NKCC2 antibody presented here is directed against amino acids 91–106 in rat NKCC2 encompassing phosphorylated threonines Thr^{96} and Thr^{101}. The amino acid sequence is highly conserved between the three cotransporters and since the antibody recognizes epitopes in the apical membranes of MD/TAL cells, basolateral domains of the parotid gland as well as an epitope in the apical domains of DCT cells, it seems able to recognize the phosphorylated forms of both NKCC2, NKCC1, and NCC. Although the antibody labels the apical domains of the DCT where NCC is found by immunohistochemistry, quantification of NCC phosphorylation is not possible by immunoblotting, since the antibody has a much higher affinity for p-NKCC2 as evaluated by immunohistochemistry.

A significant increase in phosphorylated NKCC2 was seen in response to an rGH injection. The increase in NKCC2 phosphorylation coincided with an increased reabsorption of electrolytes and water after rGH injection. Gimenez and Forbush (15) provided evidence for the involvement of Thr^{96}, Thr^{101}, and Thr^{114} in the regulation of NKCC2 cotransport

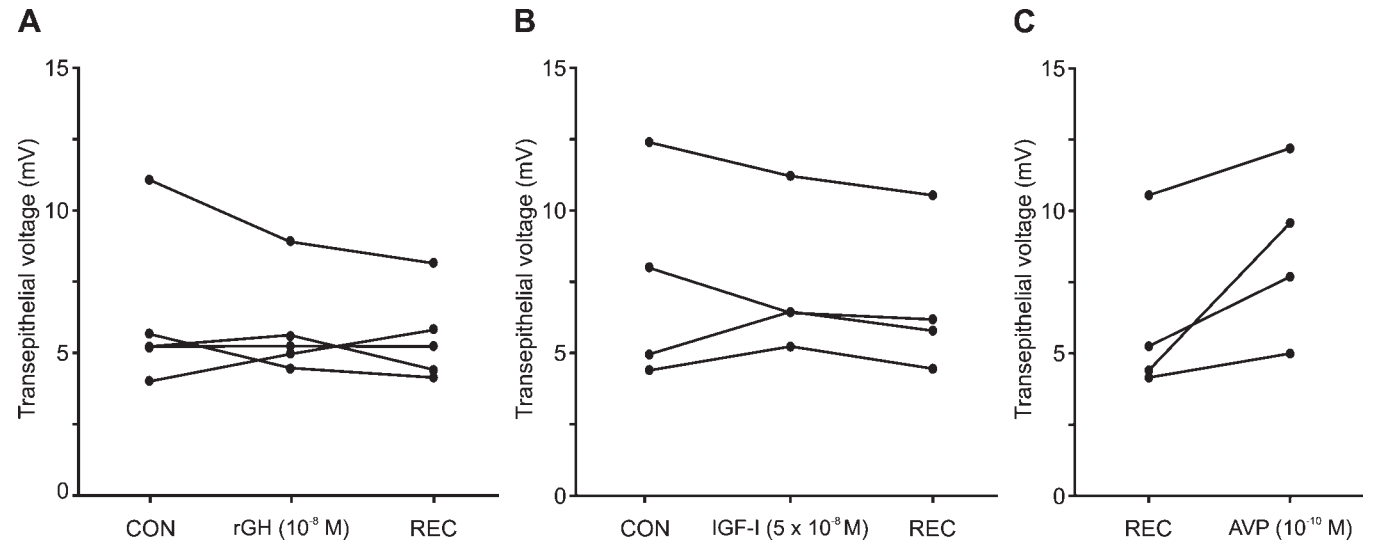

Fig. 8. Transepithelial voltage (V_{te}) was measured in isolated microperfused mTALs. *A*: changes in V_{te} in response to peritubular addition of 10^{-8} M rGH. *B*: changes in V_{te} in response to peritubular addition of 5×10^{-8} M IGF-I. Individual results obtained with 5 (rGH) or 4 (IGF-I) independent tubules are displayed. Each tubule was studied during 3 successive periods [control (CON), experimental (rGH or IGF-I), and recovery (REC)]. *C*: changes in V_{te} in response to peritubular addition of 10^{-10} M AVP. Lines connect paired measurements made in same tubule. Mean values of V_{te} appear in text.

activity during exposure to hypertonic media in *Xenopus laevis* oocytes. They found that deletion of the three phosphorylation sites on NKCC2 completely abolished the increased ion transport normally observed during exposure to hypertonic media. However, as both the interstitial and luminal osmolality in the ISOM changes in response to hydration status, it is difficult to envision the effect of these phosphorylations in response to hypertonicity in the mammalian kidney. Results from mice (16) and those of the present study show a low level of NKCC2 phosphorylation during basal conditions in the mTAL (ISOM). This indicates that the basal activity of NKCC2 is enough to maintain its function in the kidney under baseline conditions. Assuming that phosphorylation of NKCC2 in the ISOM will increase net transport rate of NKCC2, increased transepithelial transport of NaCl and to some extent K^+ into the interstitium is expected. This could account for the increased reabsorption of electrolytes observed in the rGH-injected groups. An increased transport rate of NKCC2 in the mTAL would also enhance the osmotic driving force into the interstitium, thus augmenting water removal from the descending thin limbs and the collecting ducts. Since no regulation of AQP2 in the collecting duct and no change in the estimated proximal tubular water reabsorption were found in response to rGH administration, the reduced urinary volume and increased urine osmolality observed after rGH treatment appear to be entirely dependent on an increase in the osmotic driving force for water reabsorption.

From the data presented here, one cannot exclude a role for NCC in the GH-mediated antinatriuresis and antidiuresis. Due to the limitations of the antibody used (i.e., low affinity for the epitope in the DCT), it was not possible to evaluate whether phosphorylation of NCC changes in response to GH administration. Recent evidence suggests that phosphorylation of NCC greatly affects transport rate in the oocyte expression system (48). If NCC is activated in our experiments, this would contribute to the increased NaCl reabsorption and to the increased water reabsorption, by decreasing electrolyte delivery to the collecting duct (i.e., increase osmotic driving force).

Regulation of NKCC2 and NCC phosphorylation is mediated by two serine/threonine kinases, Ste20-related proline alanine-rich kinase (SPAK) and oxidative stress response kinase (OSR1). The kinases have recently been linked to several key processes including regulation of cation-coupled chloride transport (42). Upstream kinases directly interacting with SPAK and OSR1, the so-called "with no lysine (K)" kinases, termed WNK kinases (42), have also been shown to play important roles in renal electrolyte transport (64). The signaling pathway mediating rGH-induced phosphorylation of NKCC2 may be speculated to include activation of one or several of these kinases.

Immunogold electron microscopy was used to determine the exact subcellular localization of both NKCC2 (phosphorylated and nonphosphorylated) as well as the phosphorylated fraction of NKCC2. Labeling for NKCC2 was found in intracellular vesicles and in the apical membrane as previously described (45), whereas immunogold labeling for the phosphorylated form of NKCC2 was restricted almost entirely to the apical plasma membrane. This suggests that either phosphorylation of NKCC2 is necessary for membrane insertion, as with the AQP2 water channel (44), or that NKCC2 is only phosphorylated while in the membrane. Gimenez and Forbush (16) noted that the phosphorylation level of NKCC2, and membrane targeting, appeared to work independently, since the vasopressin-induced increase in NKCC2 phosphorylation exceeded the level of protein translocation. Additionally, cAMP administration has recently been reported to directly stimulate shuttling of NKCC2 (47), while the effect on NKCC2 phosphorylation level remains unknown. In the present study, no change in density of NKCC2 in the apical plasma membrane was seen after rGH administration. This may indicate that rGH injections did not lead to increased abundance of NKCC2 in the plasma membrane. However, the possibility exists that the apical surface area of the mTAL cells is increased following rGH injections resulting in an increased number of NKCC2 molecules facing the luminal fluid, despite no detectable changes in the density of NKCC2 molecules within the membrane.

Both the GH and IGF-I receptor have been localized to the TAL (6, 35), suggesting that the increase in phosphorylation of NKCC2 seen after rGH injections could be mediated by direct action of rGH or indirectly through IGF-1. Using isolated perfused mTAL segments, we tested whether peritubular rGH addition directly stimulates NKCC2 transport activity. However, no change in V_{te} was observed. Thus the effects of rGH injections most likely rely on intermediate signaling pathways. The classic secondary signaling pathway of GH is through stimulation of IGF-I production. However, the experimental conditions (duration and rGH dose) were chosen to avoid an increased systemic IGF-I concentration, and the total plasma IGF-I concentration was unchanged between the groups. Thus the observed renal effects cannot simply be ascribed to changes in total systemic IGF-I concentration. IGF-I can also be produced and act locally, in response to GH administration (5, 51). In the present study, rGH injections resulted in increased IGF-I mRNA content in the CTX/OSOM, but not in ISOM or IM, suggesting an increased local cortical IGF-I production. Therefore, we could not rule out that local IGF-I production may mediate the effects of GH in the mTAL, assuming that IGF-I produced in CTX/OSOM can act in the ISOM. However, peritubular exposure of isolated perfused mTAL segments to IGF-I did not change the V_{te}, suggesting that IGF-I does not influence the transport rate of NKCC2, as would be expected if IGF-I induced phosphorylation of NKCC2. It should be noted that the observation of increased NKCC2 protein abundance in CTX/OSOM, but not in ISOM, coincides with increased amount of IGF-I mRNA found in CTX/OSOM, although no causal relationship can be documented.

NKCC2 has previously been shown to be phosphorylated in the mTAL after stimulation by AVP. Therefore, the effects seen in this study could be mediated by an increased plasma AVP concentration, if injection of rGH by an unknown mechanism results in increased plasma AVP concentrations. The mTAL have a high sensitivity to vasopressin, and net reabsorption of NaCl is significantly stimulated by the hormone, whereas the cTAL does not change NaCl transport in the presence of AVP (65). A similar relationship is observed in mice after acute vasopressin administration, where an increase in the phosphorylation of NKCC2 is observed in the mTAL, while the cTAL maintains a high basal level of NKCC2 phosphorylation, that is not altered after addition of AVP (16). The same could be observed in this experiment; however, as phosphorylation of Ser^{256} on AQP2 and changes in the sub-

cellular distribution of the channel are a hallmark of vasopressin action (7, 13, 46, 66), and since no changes were seen in the phosphorylation level of AQP2 or in the degree of apical targeting of AQP2, it seems unlikely that rGH injection induces an increase in plasma AVP concentration.

Insulin has been shown to increase chloride flux in the mTAL and could therefore contribute to the observed effects in this study (29). However, no change in insulin levels was observed, which is in good agreement with an earlier study of rats made diabetic by partial depancreatization. In these animals, GH still induced significant decreases in urinary sodium and potassium excretion, supporting that the antinatriuretic effect of GH is insulin independent (18). Thus at present the signaling pathways leading from rGH injection to increased phosphorylation of NKCC2 in the ISOM cannot be identified further.

The acute antinatriuretic and antidiuretic effects of GH, in conjunction with the pulsatile secretion pattern of GH from pituitary somatrophs, suggest a possible role for GH in the circadian variations of urinary electrolyte and water excretion/urinary concentration. This becomes apparent in perfused rat kidneys, where GH accelerated volume absorption was observed at concentrations as low as 3.5 nM, with half-maximal effect at 12 nM. The authors note that this is within the range of the GH concentrations achieved during episodic GH surges (62). Earlier studies have shown that a subcutaneous injection of 2–4 mg hGH induces a progressive incline in plasma hGH concentration during the first hour in female rats, a maximal serum concentration is reached after 2 h with a decline after ~4 h, following a bell-shaped curve (33). In female rats, episodic surges can reach as much as 3.64×10^{-8} M GH (9, 55), suggesting that the dose used in this study results in the expected physiological level obtained during a GH peak in female rats, although for a prolonged period of time. Despite the clear effect on NKCC2 phosphorylation documented in this study, the acute effects of rGH do not appear to be directly mediated by the hormone acting on the mTAL. However, distinct increases in renal sodium and water reabsorption are observed, suggesting a perhaps more central role for GH in renal electrolyte and water homeostasis.

ACKNOWLEDGMENTS

The skillful technical assistance of G. Kall, Z. Nikrozi, L. V. Holbech, H. Hoyer, I. M. Paulsen, I. M. Jalk, K. Thomsen, P. Plougmann, K. Mathiassen, and K. Nyborg is gratefully acknowledged. The authors thank Dr. M. A. Knepper for generously providing an anti-NKCC2 antibody. D. Eladari and A. Doucet are thanked for very helpful discussions.

GRANTS

This study was supported by grants from the Danish National Research Foundation (Danmarks Grundforskningsfond), the Novo-Nordisk Foundation, Aarhus University Research Foundation, the Margrethe Moller Foundation, the Consul Johannes Fogh-Nielsen's and Ms. Ella Fogh-Nielsen's Foundation, the Helga and Peter Kornings Foundation, the Edith Waagens and Frode Waagens Foundation, King Christian 10th Foundation, Institut National de la Santé et de la Recherche Médicale, and the renal phenotyping facility (Institut des Cordeliers).

REFERENCES

1. **Barton JS, Hindmarsh PC, Preece MA, Brook CG.** Blood pressure and the renin-angiotensin-aldosterone system in children receiving recombinant human growth hormone. *Clin Endocrinol (Oxf)* 38: 245–251, 1993.
2. **Bergenstal DM, Lipsett MB.** Metabolic effects of human growth hormone and growth hormone of other species in man. *J Clin Endocrinol Metab* 20: 1247–1435, 1960.
3. **Biglieri E, Watlington C, Forsham P.** Sodium retention with human growth hormone and its subfractions. *J Clin Endocrinol Metab* 21: 361–370, 1961.
4. **Binnerts A, Swart GR, Wilson JH, Hoogerbrugge N, Pols HA, Birkenhager JC, Lamberts SW.** The effect of growth hormone administration in growth hormone deficient adults on bone, protein, carbohydrate and lipid homeostasis, as well as on body composition. *Clin Endocrinol (Oxf)* 37: 79–87, 1992.
5. **Bortz JD, Rotwein P, DeVol D, Bechtel PJ, Hansen VA, Hammerman MR.** Focal expression of insulin-like growth factor I in rat kidney collecting duct. *J Cell Biol* 107: 811–819, 1988.
6. **Chin E, Zhou J, Bondy C.** Anatomical relationships in the patterns of insulin-like growth factor (IGF)-I, IGF binding protein-1, and IGF-I receptor gene expression in the rat kidney. *Endocrinology* 130: 3237–3245, 1992.
7. **Christensen BM, Zelenina M, Aperia A, Nielsen S.** Localization and regulation of PKA-phosphorylated AQP2 in response to V(2)-receptor agonist/antagonist treatment. *Am J Physiol Renal Physiol* 278: F29–F42, 2000.
8. **De Zegher F, Devlieger H, Veldhuis JD.** Properties of growth hormone and prolactin hypersecretion by the human infant on the day of birth. *J Clin Endocrinol Metab* 76: 1177–1181, 1993.
9. **Eden S.** Age- and sex-related differences in episodic growth hormone secretion in the rat. *Endocrinology* 105: 555–560, 1979.
10. **Epstein S, Le Roith D, Rabkin R.** The effect of different preparations of human growth hormone on plasma renin activity in normal males. *J Clin Endocrinol Metab* 42: 390–392, 1976.
11. **Feraille E, Rousselot M, Rajerison R, Favre H.** Effect of insulin on Na^+,K^+-ATPase in rat collecting duct. *J Physiol* 488: 171–180, 1995.
12. **Flemmer AW, Gimenez I, Dowd BF, Darman RB, Forbush B.** Activation of the Na-K-Cl otransporter NKCC1 detected with a phospho-specific antibody. *J Biol Chem* 277: 37551–37558, 2002.
13. **Fushimi K, Sasaki S, Marumo F.** Phosphorylation of serine 256 is required for cAMP-dependent regulatory exocytosis of the aquaporin-2 water channel. *J Biol Chem* 272: 14800–14804, 1997.
14. **Garvin JL, Knepper MA.** Bicarbonate and ammonia transport in isolated perfused rat proximal straight tubules. *Am J Physiol Renal Fluid Electrolyte Physiol* 253: F277–F281, 1987.
15. **Gimenez I, Forbush B.** Regulatory phosphorylation sites in the N-terminus of the renal Na-K-Cl cotransporter (NKCC2). *Am J Physiol Renal Physiol* 289: F1341–F1345, 2005.
16. **Gimenez I, Forbush B.** Short-term stimulation of the renal Na-K-Cl cotransporter (NKCC2) by vasopressin involves phosphorylation and membrane translocation of the protein. *J Biol Chem* 278: 26946–26951, 2003.
17. **Giordano M, DeFronzo RA.** Acute effect of human recombinant insulin-like growth factor I on renal function in humans. *Nephron* 71: 10–15, 1995.
18. **Glafkides CM, Bennett LL.** Reduction of urinary sodium and potassium of diabetic rats produced by hypophyseal growth hormone. *Proc Soc Exp Biol Med* 77: 524–526, 1951.
19. **Good DW, Knepper MA, Burg MB.** Ammonia and bicarbonate transport by thick ascending limb of rat kidney. *Am J Physiol Renal Fluid Electrolyte Physiol* 247: F35–F44, 1984.
20. **Gronbaek H, Nielsen B, Schrijvers B, Vogel I, Rasch R, Flyvbjerg A.** Inhibitory effects of octreotide on renal and glomerular growth in early experimental diabetes in mice. *J Endocrinol* 172: 637–643, 2002.
21. **Hansen TK, Moller J, Thomsen K, Frandsen E, Dall R, Jorgensen JO, Christiansen JS.** Effects of growth hormone on renal tubular handling of sodium in healthy humans. *Am J Physiol Endocrinol Metab* 281: E1326–E1332, 2001.
22. **Hayes FJ, Fiad TM, McKenna TJ.** Activity of the renin-angiotensin-aldosterone axis is dependent on the occurrence of edema in growth hormone (GH)-deficient adults treated with GH. *J Clin Endocrinol Metab* 82: 322–323, 1997.
23. **Hirschberg R, Brunori G, Kopple JD, Guler HP.** Effects of insulin-like growth factor I on renal function in normal men. *Kidney Int* 43: 387–397, 1993.
24. **Hizuka N, Takano K, Asakawa K, Fukuda I, Sukegawa I, Shizume K, Demura H.** Single sc administration of insulin-like growth factor I (IGF-I) in normal men. *Adv Exp Med Biol* 293: 105–112, 1991.

25. **Ho KY, Weissberger AJ.** The antinatriuretic action of biosynthetic human growth hormone in man involves activation of the renin-angiotensin system. *Metabolism* 39: 133–137, 1990.
26. **Honeyman TW, Goodman HM, Fray JC.** The effects of growth hormone on blood pressure and renin secretion in hypophysectomized rats. *Endocrinology* 112: 1613–1617, 1983.
27. **Ikkos D, Luft R, Sjogren B.** Body water and sodium in patients with acromegaly. *J Clin Invest* 33: 989–994, 1954.
28. **Isaksson OGP, Jansson J, Gause IAM.** Growth hormone stimulates longitudinal bone growth directly. *Science* 216: 1237–1239, 1982.
29. **Ito O, Kondo Y, Takahashi N, Omata K, Abe K.** Role of calcium in insulin-stimulated NaCl transport in medullary thick ascending limb. *Am J Physiol Renal Fluid Electrolyte Physiol* 269: F236–F241, 1995.
30. **Jensen LJN, Denner L, Schrijvers BF, Tilton RG, Rasch R, Flyvbjerg A.** Renal effects of a neutralising RAGE-antibody in long-term streptozotocin-diabetic mice. *J Endocrinol* 188: 493, 2006.
31. **Johannsson G, Sverrisdottir YB, Ellegard L, Lundberg PA, Herlitz H.** GH increases extracellular volume by stimulating sodium reabsorption in the distal nephron and preventing pressure natriuresis. *J Clin Endocrinol Metab* 87: 1743–1749, 2002.
32. **Jorgensen KD.** Comparison of the pharmacological properties of pituitary and biosynthetic human growth hormone. Demonstration of antinatriuretic/antidiuretic and barbital sleep effects of human growth hormone in rats. *Acta Endocrinol* 114: 124–131, 1987.
33. **Jorgensen PH, Bang C, Andreassen TT, Flyvbjerg A, Orskov H.** Dose response study of the effect of growth hormone on mechanical properties of skin graft wounds. *J Surg Res* 58: 295–301, 1995.
34. **Kim GH, Ecelbarger CA, Mitchell C, Packer RK, Wade JB, Knepper MA.** Vasopressin increases Na-K-2Cl cotransporter expression in thick ascending limb of Henle's loop. *Am J Physiol Renal Physiol* 276: F96–F103, 1999.
35. **Lobie PE, Garcia-Aragon J, Wang BS, Baumbach WR, Waters MJ.** Cellular localization of the growth hormone binding protein in the rat. *Endocrinology* 130: 3057–3065, 1992.
36. **Lockett MF, Nail B.** A comparative study of the renal actions of growth and lactogenic hormones in rats. *J Physiol* 180: 147–156, 1965.
37. **Marcus R, Butterfield G, Holloway L, Gilliland L, Baylink DJ, Hintz RL, Sherman BM.** Effects of short term administration of recombinant human growth hormone to elderly people. *J Clin Endocrinol Metab* 70: 519–527, 1990.
38. **Maunsbach A.** Embedding of cells and tissues for ultrastructural and immunocytochemical analysis. In: *Cell Biology. A Laboratory Handbook*, edited by Celis JE. San Diego, CA: Academic, 1994, p. 117–125.
39. **Miller SB, Rotwein P, Bortz JD, Bechtel PJ, Hansen VA, Rogers SA, Hammerman MR.** Renal expression of IGF I in hypersomatotropic states. *Am J Physiol Renal Fluid Electrolyte Physiol* 259: F251–F257, 1990.
40. **Moller J, Jorgensen JO, Moller N, Hansen KW, Pedersen EB, Christiansen JS.** Expansion of extracellular volume and suppression of atrial natriuretic peptide after growth hormone administration in normal man. *J Clin Endocrinol Metab* 72: 768–772, 1991.
41. **Moller J, Moller N, Frandsen E, Wolthers T, Jorgensen JO, Christiansen JS.** Blockade of the renin-angiotensin-aldosterone system prevents growth hormone-induced fluid retention in humans. *Am J Physiol Endocrinol Metab* 272: E803–E808, 1997.
42. **Moriguchi T, Urushiyama S, Hisamoto N, Iemura Si Uchida S, Natsume T, Matsumoto K, Shibuya H.** WNK1 regulates phosphorylation of cation-chloride-coupled cotransporters via the STE20-related kinases, SPAK and OSR1. *J Biol Chem* 280: 42685–42693, 2005.
43. **Nielsen S, DiGiovanni SR, Christensen EI, Knepper MA, Harris HW.** Cellular and subcellular immunolocalization of vasopressin-regulated water channel in rat kidney. *Proc Natl Acad Sci USA* 90: 11663–11667, 1993.
44. **Nielsen S, Frokiaer J, Marples D, Kwon TH, Agre P, Knepper MA.** Aquaporins in the kidney: from molecules to medicine. *Physiol Rev* 82: 205–244, 2002.
45. **Nielsen S, Maunsbach AB, Ecelbarger CA, Knepper MA.** Ultrastructural localization of Na-K-2Cl cotransporter in thick ascending limb and macula densa of rat kidney. *Am J Physiol Renal Physiol* 275: F885–F893, 1998.
46. **Nishimoto G, Zelenina M, Li D, Yasui M, Aperia A, Nielsen S, Nairn AC.** Arginine vasopressin stimulates phosphorylation of aquaporin-2 in rat renal tissue. *Am J Physiol Renal Physiol* 276: F254–F259, 1999.
47. **Ortiz PA.** cAMP increases surface expression of NKCC2 in rat thick ascending limbs: role of VAMP. *Am J Physiol Renal Physiol* In press.
48. **Pacheco-Alvarez D, San Cristobal P, Meade P, Moreno E, Vazquez N, Munoz E, Diaz A, Juarez ME, Gimenez I, Gamba G.** The Na-Cl cotransporter is activated and phosphorylated at the amino terminal domain upon intracellular chloride depletion. *J Biol Chem* In press.
49. **Pietrobelli DJ, Akopian M, Olivieri AO, Renauld A, Garrido D, Artese R, Feldstein CA.** Altered circadian blood pressure profile in patients with active acromegaly. Relationship with left ventricular mass and hormonal values. *J Hum Hypertens* 15: 601–605, 2001.
50. **Quigley R, Baum M.** Effects of growth hormone and insulin-like growth factor I on rabbit proximal convoluted tubule transport. *J Clin Invest* 88: 368–374, 1991.
51. **Rogers SA, Miller SB, Hammerman MR.** Growth hormone stimulates IGF I gene expression in isolated rat renal collecting duct. *Am J Physiol Renal Fluid Electrolyte Physiol* 259: F474–F479, 1990.
52. **Rosen T, Bosaeus I, Tolli J, Lindstedt G, Bengtsson BA.** Increased body fat mass and decreased extracellular fluid volume in adults with growth hormone deficiency. *Clin Endocrinol (Oxf)* 38: 63–71, 1993.
53. **Salomon F, Cuneo RC, Hesp R, Sonksen PH.** The effects of treatment with recombinant human growth hormone on body composition and metabolism in adults with growth hormone deficiency. *N Engl J Med* 321: 1797–1803, 1989.
54. **Satozawa N, Takezawa K, Miwa T, Takahashi S, Hayakawa M, Ooka H.** Differences in the effects of 20 K- and 22 K-hGH on water retention in rats. *Growth Horm IGF Res* 10: 187–192, 2000.
55. **Saunders A, Terry LC, Audet J, Brazeau P, Martin JB.** Dynamic studies of growth hormone and prolactin secretion in the female rat. *Neuroendocrinology* 21: 193–203, 1976.
56. **Simone PG, Solomon S.** Aldosterone and growth hormone: influence of diet and hypophysectomy on rat renal response. *Proc Soc Exp Biol Med* 133: 786–789, 1970.
57. **Sondergaard M, Dagnaes-Hansen F, Flyvbjerg A, Jensen TG.** Normalization of growth in hypophysectomized mice using hydrodynamic transfer of the human growth hormone gene. *Am J Physiol Endocrinol Metab* 285: E427–E432, 2003.
58. **Stein JD Jr, Bennett LL, Batts AA, Li CH.** Sodium, potassium, and chloride retention produced by growth hormone in the absence of the adrenals. *Am J Physiol* 171: 587–591, 1952.
59. **Thomsen K.** Lithium clearance: a new method for determining proximal and distal tubular reabsorption of sodium and water. *Nephron* 37: 217–223, 1984.
60. **Thomsen K, Shalmi M, Olesen OV.** Effect of low dietary sodium and potassium on lithium clearance in rats. *Miner Electrolyte Metab* 19: 91–98, 1993.
61. **Thomsen K, Shirley DG.** The validity of lithium clearance as an index of sodium and water delivery from the proximal tubules. *Nephron* 77: 125–138, 1997.
62. **Welbourne TC, Cronin MJ.** Growth hormone accelerates tubular acid secretion. *Am J Physiol Regul Integr Comp Physiol* 260: R1036–R1042, 1991.
63. **Whitney JE, Bennett LL, Li CH.** Reduction of urinary sodium and potassium produced by hypophyseal growth hormone in normal female rats. *Proc Soc Exp Biol Med* 79: 584–587, 1952.
64. **Wilson FH, Disse-Nicodeme S, Choate KA, Ishikawa K, Nelson-Williams C, Desitter I, Gunel M, Milford DV, Lipkin GW, Achard JM, Feely MP, Dussol B, Berland Y, Unwin RJ, Mayan H, Simon DB, Farfel Z, Jeunemaitre X, Lifton RP.** Human hypertension caused by mutations in WNK kinases. *Science* 293: 1107–1112, 2001.
65. **Wittner M, di Stefano A, Wangemann P, Nitschke R, Greger R, Bailly C, Amiel C, Roinel N, de Rouffignac C.** Differential effects of ADH on sodium, chloride, potassium, calcium and magnesium transport in cortical and medullary thick ascending limbs of mouse nephron. *Pflügers Arch* 412: 516–523, 1988.
66. **Zelenina M, Christensen BM, Palmer J, Nairn AC, Nielsen S, Aperia A.** Prostaglandin E_2 interaction with AVP: effects on AQP2 phosphorylation and distribution. *Am J Physiol Renal Physiol* 278: F388–F394, 2000.